Article

Cell Reports

Activation of Astrocytic μ-Opioid Receptor Causes Conditioned Place Preference

Graphical Abstract

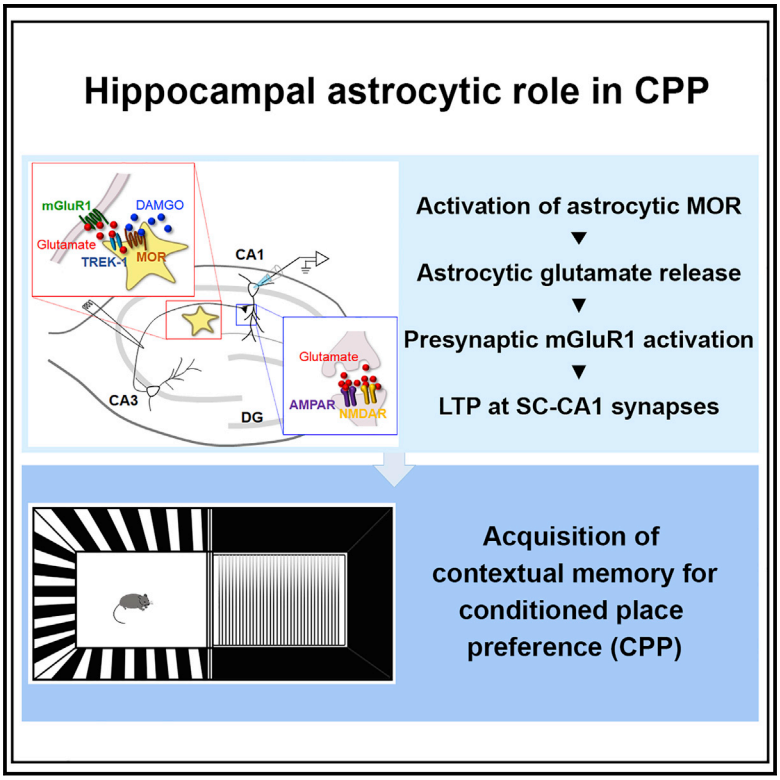

Highlights

- Hippocampal astrocytic μ-opioid receptor (MOR) activation drives conditioned place preference (CPP)
- Astrocytic MOR activation enhances synaptic plasticity at the Schaffer collateral pathway
- Chemogenetic activation of astrocytic Gi-DREADD recapitulates MOR-mediated LTP and CPP

Authors

Min-Ho Nam, Kyung-Seok Han, Jaekwang Lee, ..., Se-Young Choi, Yong Chul Bae, C. Justin Lee

Correspondence

ycbae@knu.ac.kr (Y.C.B.), cjl@ibs.re.kr (C.J.L.)

In Brief

Nam et al. demonstrate that activation of hippocampal astrocytic μ-opioid receptor causes glutamate release, which increases the release probability by neuronal presynaptic mGluR1 activation and potentiates synaptic plasticity at the SC-CA1 pathway. This enhanced synaptic transmission and synaptic plasticity account for the acquisition of memory associated with CPP.

Nam et al., 2019, Cell Reports *28*, 1154–1166
July 30, 2019
https://doi.org/10.1016/j.celrep.2019.06.071

CellPress

OPEN ACCESS
CellPress

Cell Reports
Article

Activation of Astrocytic μ-Opioid Receptor Causes Conditioned Place Preference

Min-Ho Nam,[1,2,12] Kyung-Seok Han,[1,3,12] Jaekwang Lee,[1,12] Woojin Won,[1,4,5] Wuhyun Koh,[1,3,5] Jin Young Bae,[6] Junsung Woo,[1,3] Jayoung Kim,[1] Elliot Kwong,[1] Tae-Yong Choi,[7] Heejung Chun,[1,5] Seung Eun Lee,[9] Sang-Bum Kim,[10] Ki Duk Park,[3,8,11] Se-Young Choi,[7] Yong Chul Bae,[6,*] and C. Justin Lee[1,3,5,13,*]

[1]Center for Neuroscience, Korea Institute of Science and Technology (KIST), Seoul 02792, Korea
[2]Department of Science in Korean Medicine, Graduate School, Kyung Hee University, Seoul 02447, Korea
[3]Department of Neuroscience, Division of Bio-Medical Science & Technology, KIST School, Korea University of Science and Technology, Seoul 02792, Korea
[4]KU-KIST Graduate School of Converging Science and Technology, Korea University, Seoul 02841, Korea
[5]Center for Cognition and Sociality, Institute for Basic Science, Daejeon 34126, Korea
[6]Department of Anatomy and Neurobiology, School of Dentistry, Kyungpook National University, Daegu 41940, Korea
[7]Department of Physiology and Dental Research Institute, Seoul National University School of Dentistry, Seoul 03080, Korea
[8]KHU-KIST Department of Converging Science and Technology, Kyung Hee University, Seoul 02447, Korea
[9]Virus Facility, Research Animal Resource Center, KIST, Seoul 02792, Korea
[10]New Drug Development Center, Daegu-Gyeongbuk Medical Innovation Foundation, Daegu 41061, Korea
[11]Convergence Research Center for Diagnosis, Treatment and Care System of Dementia, KIST, Seoul 02792, Korea
[12]These authors contributed equally
[13]Lead Contact
*Correspondence: ycbae@knu.ac.kr (Y.C.B.), cjl@ibs.re.kr (C.J.L.)
https://doi.org/10.1016/j.celrep.2019.06.071

SUMMARY

The underlying mechanisms of how positive emotional valence (e.g., pleasure) causes preference of an associated context is poorly understood. Here, we show that activation of astrocytic μ-opioid receptor (MOR) drives conditioned place preference (CPP) by means of specific modulation of astrocytic MOR, an exemplar endogenous Gi protein-coupled receptor (Gi-GPCR), in the CA1 hippocampus. Long-term potentiation (LTP) induced by a subthreshold stimulation with the activation of astrocytic MOR at the Schaffer collateral pathway accounts for the memory acquisition to induce CPP. This astrocytic MOR-mediated LTP induction is dependent on astrocytic glutamate released upon activation of the astrocytic MOR and the consequent activation of the presynaptic mGluR1. The astrocytic MOR-dependent LTP and CPP were recapitulated by a chemogenetic activation of astrocyte-specifically expressed Gi-DREADD hM4Di. Our study reveals that the transduction of inhibitory Gi-signaling into augmented excitatory synaptic transmission through astrocytic glutamate is critical for the acquisition of contextual memory for CPP.

INTRODUCTION

Memories are often associated with emotions of positive (e.g., joy and pleasure) or negative valence (e.g., fear and anger). Much research has focused on the latter category, of which contextual fear memory is an example. It has been reported that such memories cause avoidance of their associated contexts by means of a circuit connecting the basolateral amygdala to the hippocampus (Amano et al., 2011; Phillips and LeDoux, 1992; Redondo et al., 2014). By contrast, the molecular and cellular mechanism of how the memory associated with emotions of positive valance causes reward process has remained elusive; prior research has, however, divided it into three components: liking and/or pleasure, learning and/or memory, and wanting and/or motivation (Kringelbach and Berridge, 2010). Liking and/or pleasure has been considered to be mediated by endogenous opioids, such as β-endorphin and enkephalin (Belluzzi and Stein, 1977; Hennig et al., 1994), and wanting and/or motivation by dopamine (Hawkes, 1992; Wise, 2004). However, the exact mechanism of the acquisition of contextual memory associated with pleasure, which is the principal component for conditioned place preference (CPP), is poorly understood.

The hippocampus is critical to the formation of contextual memory. However, whether this capacity extends to the memory formation for CPP has remained elusive, whereas the hippocampus has been recently reported to be responsible for retrieval of CPP-associated memory (Roy et al., 2017). Meanwhile, it has been found that in the spinal cord opioid withdrawal induces long-term potentiation (LTP) in an NMDA receptor (NMDAR)-dependent and GABA-independent manner, possibly suggesting that glutamate is required for opioid-induced alteration of synaptic plasticity and opioid withdrawal (Drdla et al., 2009). In support of this idea, μ-opioid receptor (MOR) activation was shown to be partly responsible for the frequency dependence of mossy fiber LTP induction in hippocampal CA3 (Derrick and Martinez, 1994). On the other hand, it is difficult to imagine that the activation of neuronal MOR could induce NMDAR-dependent LTP because neuronal MOR, an exemplar Gi-protein coupled receptor (Gi-GPCR), usually exerts a powerful inhibitory effect (Johnson and North, 1992). Alternatively, we have recently demonstrated that astrocytes in the CA1 hippocampus exhibit

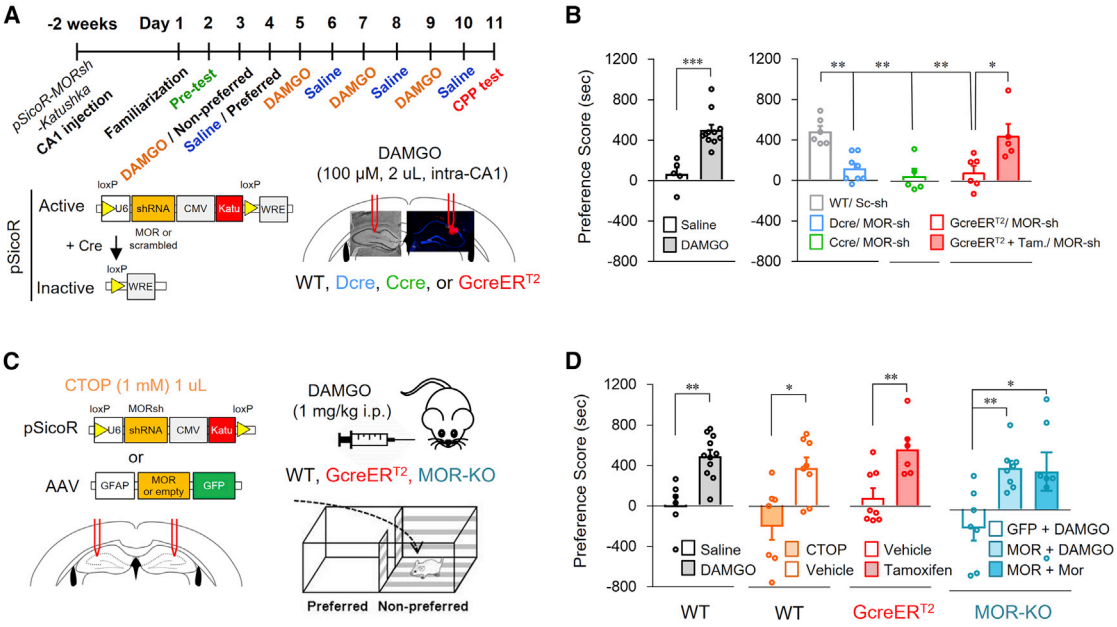

Figure 1. Activation of Astrocytic MOR Induces Conditioned Place Preference

(A) Experimental scheme of intra-CA1 DAMGO-CPP test. DAMGO and pSicoR-MOR-shRNA virus were bilaterally infused into the CA1 hippocampus.

(B) Summary bar graph of the preference score (sec) induced by intra-CA1 DAMGO infusion in each condition ($n \geq 5$ mice; *$p < 0.05$, **$p < 0.01$, ***$p < 0.001$, two-tailed Mann-Whitney test or one-way ANOVA with Tukey's multiple comparison test).

(C) Experimental scheme of i.p. DAMGO-CPP test. DAMGO was i.p. injected; viruses and CTOP were bilaterally infused into CA1 hippocampus.

(D) Summary bar graph of the preference score (sec) induced by i.p. DAMGO injection in each condition ($n \geq 6$ mice; *$p < 0.05$, **$p < 0.01$, ***$p < 0.001$, two-tailed Mann-Whitney test or one-way ANOVA with Tukey's multiple comparison test). Data are represented as mean ± SEM.

See Table S1 for detailed description about statistical analyses.

high expressions of MOR (Nam et al., 2018), whose activation induces a significant release of glutamate from astrocytes through TREK-1-containing two-pore potassium (K2P) channels (Woo et al., 2018; Woo et al., 2012). Such astrocytic glutamate has a potential to exert a noncanonical excitatory effect of Gi-GPCR onto neighboring neurons to induce LTP. Coincidentally, the possibility that glial Gi-GPCR is critical to the induction of hippocampal LTP was proposed three decades ago (Goh and Pennefather, 1989); however, it was never tested. The present study explored the hypothesis that the activation of astrocytic MOR, as an example of Gi-GPCRs, enhances synaptic transmission and plasticity of the Schaffer collateral (SC) pathway, thereby inducing the formation of contextual memory for CPP.

RESULTS

Hippocampal Astrocytic MOR Is Necessary for CPP

We first ascertained whether hippocampal astrocytic MOR is necessary for CPP (Carr et al., 1989), which requires not only a reward-based motivation but also the formation of contextual memory. It is well known that MOR activation by the systemic administration of opioids, such as morphine, induces CPP (Mucha et al., 1982). Here, we found that activation of hippocampal MOR can induce CPP by a local and bilateral infusion of a selective MOR agonist, [D-Ala2, N-MePhe4, Gly-ol]-enkephalin (DAMGO; 100 μM), into the CA1 hippocampus (Figures 1A, 1B, and S1A). To determine if the astrocytic MOR is required for the DAMGO-induced CPP, we used a cell-type-specific gene-silencing system consisting of a lentivirus carrying pSicoR- MOR short hairpin RNA (MOR-shRNA) (Nam et al., 2018), which can be cleaved by Cre recombinase from DLX-Cre (gamma-aminobutyric acid [GABA]ergic interneuronal Cre) (Stenman et al., 2003), CamKIIα-Cre (pyramidal neuronal Cre), or hGFAP-CreER^{T2} (tamoxifen-inducible astrocytic Cre) (Casper et al., 2007) mouse lines (Figures 1B and S2; Ventura et al., 2004; Woo et al., 2012). In other words, the MOR-shRNA can silence MOR expression in all cell types except for the Cre-expressing cells (Figures S1C–S1G). We found that neither interneuronal nor pyramidal neuronal MOR contributed to DAMGO-induced CPP in the CA1 hippocampus, as evidenced by the observation that CPP was abolished by MOR-shRNA injection into the CA1 of DLX-Cre and CaMKIIα-Cre mice (Figure 1B). In contrast, we found that intra-CA1 DAMGO infusion significantly induced CPP in the MOR-shRNA-injected hGFAP-CreER^{T2} mice with tamoxifen treatment (astrocyte-specific flanking of MOR-shRNA) but not in control sunflower-oil-treated hGFAP-CreER^{T2} mice (global expression of MOR-shRNA) (Figure 1B). These results indicate that activation of astrocytic MOR, but not neuronal MOR, in the dorsal CA1 hippocampus is necessary for CPP.

As DAMGO was locally infused into the hippocampal CA1 region, the possibility that MOR in other brain regions might also participate in CPP could not be ruled out. We, therefore, tested whether MOR in hippocampal astrocytes is required for

DAMGO-induced CPP when DAMGO (1 mg/kg) is administered systemically through intraperitoneal (i.p.) injection (Figure 1C). First, we observed that the systemic administration of DAMGO successfully crossed the blood-brain barrier (Figure S3) and induced CPP in WT mice (Figure 1D). To test if MOR in the dorsal hippocampus is necessary for systemic DAMGO-induced CPP, we performed the CPP experiment with DAMGO after locally and bilaterally infusing 1 μL of 1 mM D-Phe-Cys-Tyr-D-Trp-Orn-Thr-Pen-Thr-NH_2 (CTOP), a selective MOR antagonist into hippocampal CA1. We found that intra-CA1 CTOP-infusion eliminated systemic DAMGO-induced CPP, whereas control-saline-infusion did not (Figure 1D). Testing whether the astrocytic MOR in the dorsal hippocampus is required for CPP, we found that the systemic DAMGO-induced CPP was eliminated when MOR-shRNA was injected into the CA1 hippocampus of hGFAP-$CreER^{T2}$ mice; tamoxifen injection fully rescued CPP (Figure 1D). Furthermore, selective overexpression of MOR in the hippocampal astrocytes of MOR-knockout (KO) mice by the injection of the adeno-associated virus (AAV) carrying GFAP-MOR-GFP into the bilateral CA1 was sufficient to yield both DAMGO- and morphine-induced CPP (Figure 1D). This elimination of CPP by gene silencing or deletion of MOR was confirmed to be due to neither an impairment of synaptic transmission or synaptic plasticity at SC-CA1 synapse (Figure S4A) nor an impaired contextual fear memory (Figure S4B). Taken together, these results indicate that even with the systemic administration of DAMGO, which should have activated MOR in other brain regions, the astrocytic MOR in CA1 hippocampus is sufficient and necessary for CPP.

Activation of Astrocytic MOR Enhances SC-CA1 Synaptic Plasticity

We next tested if activation of astrocytic MOR is sufficient for LTP, a neural correlate of CA1 hippocampus-dependent contextual memory (Bliss and Collingridge, 1993; Penn et al., 2017; Whitlock et al., 2006), at SC-CA1 synapse. We recorded the slope of field excitatory postsynaptic potentials (fEPSPs) after performing an electrical stimulation protocol as a measure of synaptic strength in acutely prepared hippocampal slices with DAMGO treatment. We found that DAMGO treatment significantly enhanced synaptic strength with electrical stimulation of different frequencies (1 and 10 Hz, but not 100 Hz; Figures 2A–2D). This was accompanied with a significant decrease in paired pulse ratio (PPR; Figure 2E), suggesting that the enhanced synaptic strength could be attributed to increased presynaptic release of glutamate. On the other hand, DAMGO treatment alone was not enough to promote synaptic plasticity, even though it enhanced synaptic transmission (Figures 2F–2H). We also found a significant LTP induced by DAMGO treatment with a 40-Hz subthreshold stimulation; the subthreshold stimulation alone could not induce LTP (Figures 2F–2H). This DAMGO-induced LTP was blocked by treatment of CTOP, a specific MOR antagonist (Figure S5A). In addition, this DAMGO-induced LTP was attributed to astrocytic MOR, but not neuronal MOR, by means of a cell-type-specific gene silencing strategy (Figures 2I–2K). Moreover, the blockade of LTP by (2R)-amino-5-phosphonovaleric acid (APV) application (Figures 2G and 2H) indicated that the DAMGO-induced LTP was dependent on postsynaptic NMDARs. We had previously predicted that metabotropic glutamate receptor 1 (mGluR1) and NMDAR are the primary targets of astrocytically released glutamate upon activation of astrocytic Gi-GPCR (Woo et al., 2012). We found that this DAMGO-induced LTP was dependent on mGluR1 as evidenced by the absence of LTP in the mGluR1-KO mice (Figures 2G and 2H). This finding is in line with previous reports demonstrating that group 1 mGluRs contribute to LTP (Gil-Sanz et al., 2008; Neyman and Manahan-Vaughan, 2008). However, the absence of DAMGO-induced LTP in this mGluR1-KO mouse cannot be simply attributed to the absence of mGluR1 because this mouse was reported to show a reduced but not completely impaired LTP by a high-frequency stimulation (Gil-Sanz et al., 2008). In contrast, NMDAR was minimally affected by astrocytic glutamate released upon MOR activation (Figures S5B–S5E). The fEPSP results, therefore, suggest that astrocytic MOR activation is necessary for lowering the LTP threshold, possibly by means of glutamate signaling through mGluR1 that prompts NMDAR-dependent LTP. Our findings are consistent with previous reports demonstrating that morphine treatment induces synaptic potentiation *in vivo* (Yang et al., 2004) and structural plasticity in hippocampal neurons (Fakira et al., 2016; Portugal et al., 2014).

Activation of Astrocytic MOR Elicits Glutamate Release, Possibly by a Ca^{2+}-Independent Manner

According to Hebbian theory, LTP induction at SC-CA1 requires enhanced glutamatergic synaptic transmission. Because we have previously reported that activation of astrocytic Gi-GPCR, such as MOR, elicits a glutamate release *in vitro* (Woo et al., 2018; Woo et al., 2012), glutamate released from astrocytes upon activation of astrocytic MOR could be the possible transmitter that is involved in this enhancement of glutamatergic synaptic transmission. Before testing this hypothesis, we first tested if activation of astrocytic MOR indeed causes a glutamate release in an *ex vivo* condition with a recently developed glutamate sensor, iGluSnFr (Marvin et al., 2013). We virally expressed iGluSnFr specifically to astrocytes in the CA1 hippocampus using the GFAP promoter (Figure 3A). We found that DAMGO treatment elicited a robust glutamate signal in the astrocytes (Figure 3B), even in the presence of tetrodotoxin (TTX) (Figure 3C). This DAMGO-induced glutamate signal was completely blocked by a treatment with CTOP (Figure 3C). These findings indicate that astrocytes release glutamate upon MOR activation.

We also have previously reported that the astrocytic glutamate release upon activation of astrocytic Gi-GPCR including MOR could be Ca^{2+} independent (Woo et al., 2018; Woo et al., 2012). On the other hand, several reports have demonstrated that activation of astrocytic Gi-GPCR, such as $GABA_B$ and hM4Di, evoked Ca^{2+} signals (Chai et al., 2017; Durkee et al., 2019). However, astrocytic MOR has not been tested yet. Therefore, we tested if MOR activation evokes astrocytic Ca^{2+} signals with GCamP6f by using an AAV with a GFAP promoter (Figure 3D; Chen et al., 2013). We found that DAMGO treatment did not cause any increase of Ca^{2+} signals, whereas dramatic Ca^{2+} signals were elicited by treatment of TFLLR, a selective agonist for protease-activated receptor-1, which is coupled to both

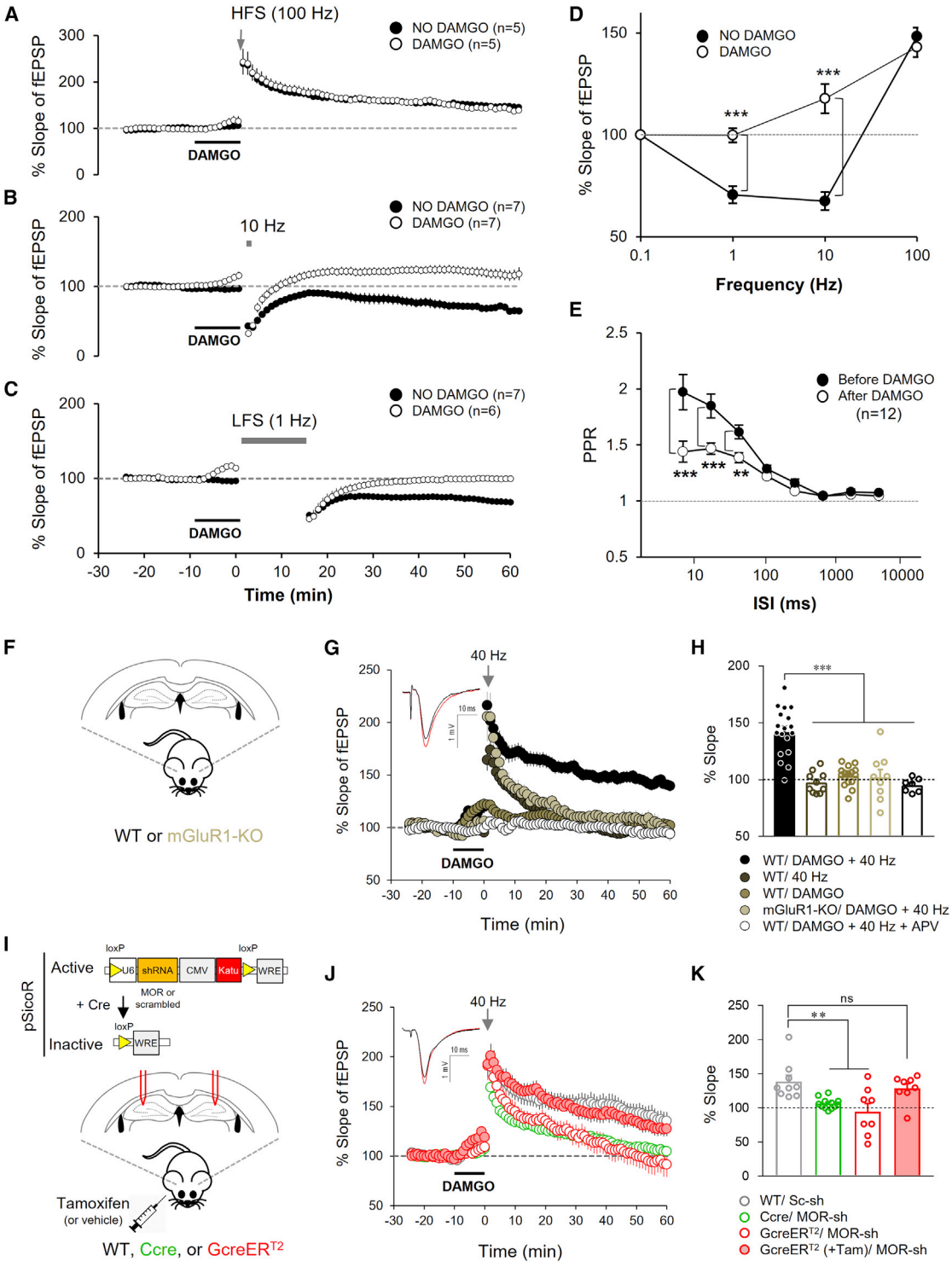

Figure 2. Activation of Astrocytic MOR Lowers LTP Threshold by Increased Presynaptic Release of Glutamate

(A–C) Time courses of the percent fEPSP slopes by high-frequency stimulation (HFS; 100 Hz; A), 10-Hz stimulation (B), or low-frequency stimulation (LFS; 1 Hz, 900 s; C). Black lines indicate 10-min DAMGO (1 μM) treatment, and arrow indicates timing of HFS. Black circles indicate slopes in the absence of DAMGO, and white circles indicate slopes in the presence of DAMGO.

(D) The percent of fEPSP by each electrical stimulation in the presence of DAMGO (white circles) or in the absence of DAMGO (black circles). The percentage of slopes of fEPSP was calculated by averaging the fEPSP of last 10 min (***$p < 0.001$, two-way ANOVA with Bonferroni's multiple comparison test).

(legend continued on next page)

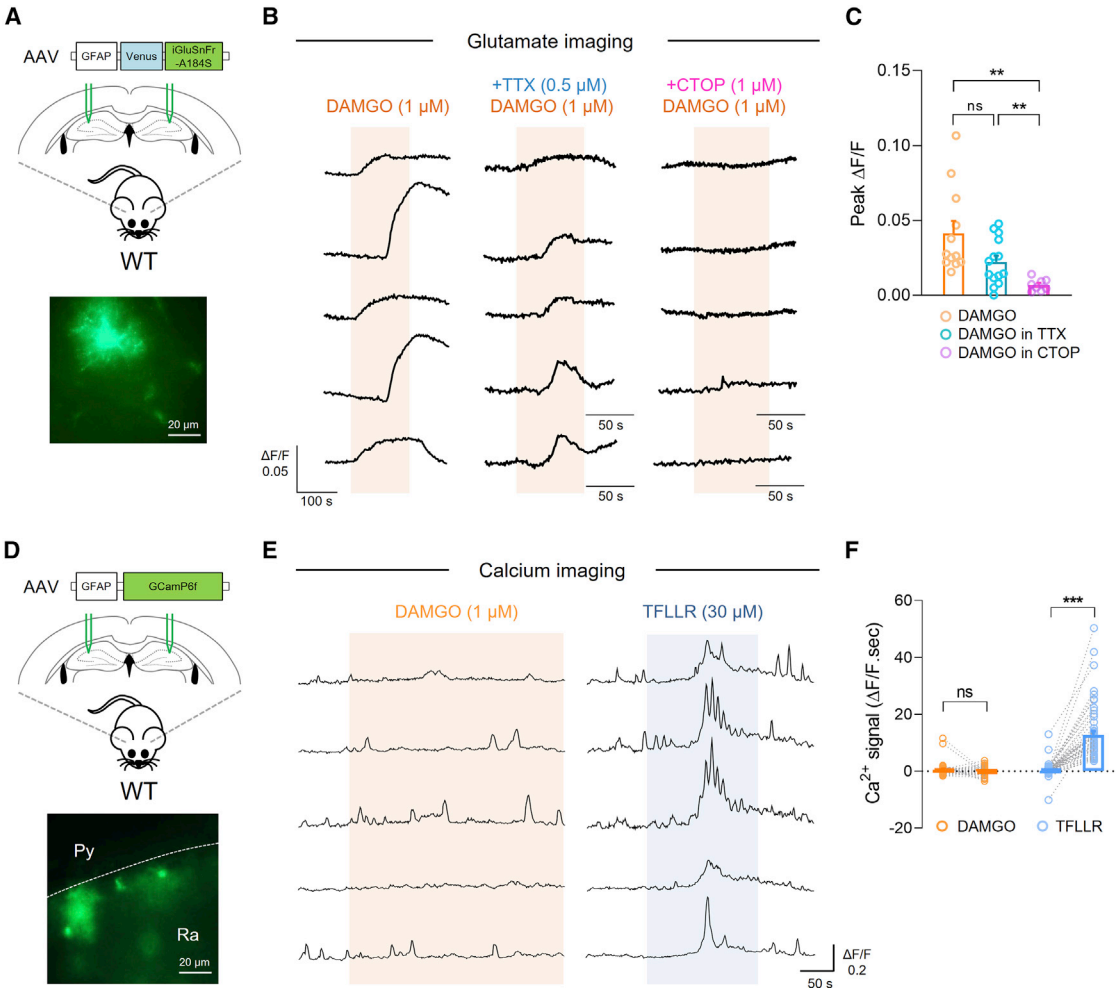

Figure 3. MOR Activation Elicits Astrocytic Glutamate Release, Possibly by a Ca^{2+}-Independent Mechanism

(A) Representative traces of glutamate signal from iGluSnFr-A184S-expressing CA1 astrocytes with DAMGO (1 μM) and TTX (0.5 μM) treatment.

(B) Representative image of iGluSnFr-A184S expression in CA1 stratum radiatum.

(C) Summary bar graph of the peak ΔF/F from each condition (n = 4 mice; **p < 0.01, Brown-Forsythe and Welch ANOVA with Games-Howell's multiple comparison test).

(D) Representative traces of calcium signals from GCamP6f-expressing CA1 astrocytes with DAMGO (1 μM) or TFLLR (30 μM) treatment.

(E) Representative image of GCamP6f expression in CA1 stratum radiatum.

(F) Summary bar graph of the peak ΔF/F from each condition (n = 4 mice; ***p < 0.001, repeated-measure two-way ANOVA with Bonferroni's multiple comparison test). Data are represented as mean ± SEM.

See Table S1 for detailed description about statistical analyses.

Gq and Gi/o proteins (Figures 3E and 3F). Consistent with our previous report (Woo et al., 2018), these results suggest that activation of astrocytic MOR elicits a glutamate release in a Ca^{2+}-independent manner. Further investigation is needed to clarify the role of Ca^{2+} in MOR-induced glutamate release in astrocytes.

Activation of Astrocytic MOR Enhances Glutamatergic Synaptic Transmission

To investigate the detailed mechanisms of how the astrocytically released glutamate causes the enhancement of glutamatergic synaptic transmission, we performed whole-cell patch clamp recordings to measure evoked excitatory postsynaptic current

(E) Summary graph of paired-pulse ratio (PPR) before (black circle) and after (white circles; n = 12) DAMGO treatment (**p < 0.01, ***p < 0.001, two-way ANOVA with Bonferroni's multiple comparison test).

(F–K) Experimental scheme of mice preparation (F and I). Time courses of the percent fEPSP slopes in each condition (G and J). Black lines indicate 10-min DAMGO (1 μM) treatment, and the arrows indicate the 40 Hz × 10 stimuli. Inset: example traces of DAMGO + 40 Hz group (G) or sc-sh group (J) before (black) and after (red) stimulation. (H and K) Summary bar graphs of the mean percent fEPSP slopes for last 10 min (n ≥ 3 mice; **p < 0.01, ***p < 0.001, ns, non-significant, one-way ANOVA with Dunnett's multiple comparison test). Data are represented as mean ± SEM.

See Table S1 for detailed description about statistical analyses.

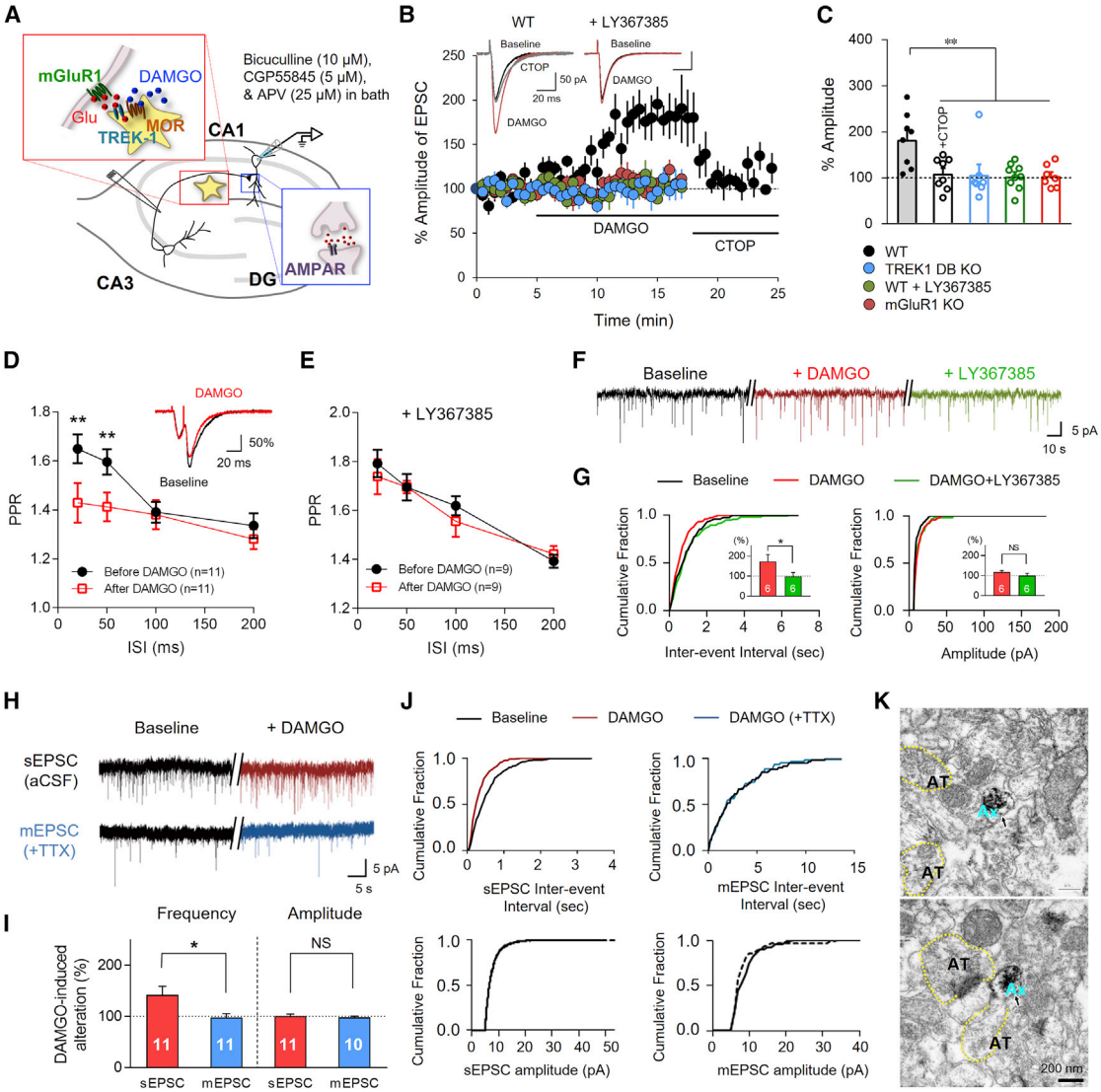

Figure 4. Astrocytic Glutamate Targets mGluR1 Localized in Presynaptic Axon Processes

(A) Mechanistic model of how astrocytic glutamate enhances synaptic transmission at SC-CA1.

(B) Time course of eEPSC amplitude by bath application of 1 μM DAMGO. Insets, representative traces from CA1 pyramidal neurons.

(C) Summary bar graph of averaged eEPSC amplitude by DAMGO for last 3 min. ($n \geq 3$ mice; $^{**}p < 0.01$, one-way ANOVA with Dunnett's multiple comparison test).

(D) Summary graph of PPR before (black) and after (red) 1 μM DAMGO treatment in the presence of bicuculline and CGP55845. Inset, representative traces with normalization of first response. ($n \geq 3$ mice; $^{**}p < 0.01$, paired two-tailed t test).

(E) Summary graph of PPR in the presence of 100 μM LY367385 (no significant difference between two groups by paired two-tailed t test).

(F) Representative traces of sEPSC with 1 μM DAMGO and 100 μM LY367385 in the presence of bicuculline and CGP55845.

(G) Summary graphs of frequency and amplitude of EPSCs ($n \geq 3$ mice; $^{*}p < 0.05$, NS, non-significant, Wilcoxon matched-pairs signed rank test).

(H) Representative traces of sEPSC (no TTX) and mEPSC (+0.5 μM TTX) with 1-μM DAMGO treatment in the presence of bicuculline and CGP55845.

(I and J) Summary graphs of frequency and amplitude of sEPSC and mEPSC (I) and the cumulative plot for inter-event interval and amplitude of sEPSC and mEPSC (J) ($n \geq 3$ mice; $^{*}p < 0.05$, NS, non-significant, Mann-Whitney test or unpaired two-tailed t test).

(K) Electron microscopic image of subcellular localization of mGluR1 in axonal processes (Ax). AT indicates axon terminals. Data are represented as mean ± SEM. See Table S1 for detailed description about statistical analyses.

(eEPSC) from CA1 pyramidal neurons. The measurements were obtained in the presence of APV to exclude any confounding contribution of synaptic plasticity. We first tested whether GABA-mediated disinhibition is involved in DAMGO-induced enhancement of synaptic transmission at SC-CA1, as was previously shown for dopaminergic neurons (Johnson and North, 1992). DAMGO-induced enhancement of the eEPSC was not eliminated by application of $GABA_A$ and $GABA_B$ blockers (bicuculline and CGP55845, respectively) (Figures 4A, S5F, and S5G), indicating that GABA-mediated disinhibition was not involved

and that glutamate remained as a strong candidate transmitter. The DAMGO-induced enhancement of eEPSC was blocked by the MOR antagonist CTOP (Figures 4B and 4C). This MOR-dependent enhancement of eEPSC was completely absent in TREK-1-TWIK-1 double-KO mice (Figures 4B, 4C, and S6A–S6D). In the context of a previous finding that activation of astrocytic MOR induces glutamate release by TREK-1- and TWIK-1-containing K2P channels (Woo et al., 2018), these results suggest that astrocytic glutamate is critical for DAMGO-induced enhancement of eEPSC. Consistent with our finding that mGluR1-KO mice did not exhibit DAMGO-induced LTP, the DAMGO-induced enhancement of eEPSC was completely blocked by LY367385, an mGluR1 antagonist, and in mGluR1-KO mice (Figures 4B and 4C). These findings indicate that DAMGO-induced astrocytic glutamate targets mGluR1 and consequently enhances eEPSC. This DAMGO-induced enhancement of eEPSC is pharmacologically and mechanistically distinct from the enhanced LTP; it is insensitive to NMDAR blocker, APV, and readily reversible. In contrast, DAMGO-induced LTP (e.g., DAMGO-induced enhancement of fEPSP) is sensitive to APV, and once it is induced, it is not readily reversible (e.g., synaptic plasticity). The insensitivity to APV of the DAMGO-induced enhancement of eEPSC was because the eEPSCs were recorded from patch-clamp experiments in which the membrane was held at resting membrane potential, and this in effect would have prevented the unblocking of NMDARs by Mg^{2+}. On the other hand, the sensitivity to APV of the DAMGO-induced enhancement of fEPSP was because fEPSP recording allows the membrane potential to be freely changed and this would have relieved the Mg^{2+} block to allow NMDAR activation. Such a mechanism can allow synaptic plasticity through NMDARs in response to applied stimulation even at basal frequency (e.g., not high-frequency stimulation that is typically required).

Presynaptic mGluR1 Is Responsible for the Enhanced Synaptic Transmission

To test if mGluR1 targeted by astrocytic glutamate is localized to the presynaptic or postsynaptic neuron, we measured the PPR. DAMGO treatment caused a change in the PPR that was not observed in the presence of LY367385 (Figures 4D and 4E), indicating that astrocytic glutamate released upon DAMGO treatment targets presynaptic mGluR1 and prompts the increase of glutamate release at SC-CA1. We further observed that DAMGO increased the frequency of spontaneous EPSC (sEPSC) without affecting the sEPSC amplitude; this finding was reversed by LY367385 application (Figures 4F and 4G), confirming the presynaptic localization of mGluR1. To identify the precise localization of mGluR1 in the presynaptic neuron, we recorded miniature EPSCs (mEPSCs) in the presence of TTX. In contrast to the increased sEPSC frequency and decreased PPR, DAMGO treatment did not increase the frequency of mEPSC (Figures 4H–4J). This TTX sensitivity of the increased sEPSC frequency has been extensively investigated in the past (Engelman and MacDermott, 2004) and has been associated with the localization of the presynaptic receptor, such as presynaptic α-amino-3-hydroxy-5-methyl-4-isoxazolepropionic acid (AMPA) receptors at the axon strand and along the axons, but not at the presynaptic terminals (Lee et al., 2002; Lee et al., 2004). If mGluR1 is mainly localized at the presynaptic axon terminals, then an activation of mGluR1 should have directly caused glutamate release from synaptic vesicles at the presynaptic terminals and increased the mEPSC frequency, even in the presence of TTX. Therefore, these findings suggest that mGluR1 is less likely to be localized at the presynaptic terminals.

On the other hand, mGluR1 localized at CA1 axon terminals has recently been reported (Gómez-Gonzalo et al., 2015). Therefore, we carefully examined the subcellular localization of mGluR1 by using electron microscopy in the SC pathway of hippocampus. We found that mGluR1 immunoreactivity was frequently observed in the axonal strands (30.5%, 53/174) and postsynaptic dendrites (66.7%, 116/174) but occasionally in the presynaptic axon terminals (2.9%, 5/174) (Figures 4K and S6). Thus far, our findings suggest that astrocytic glutamate activates mGluR1 expressed in axonal processes and, thereby, increases the excitability of axons, possibly by blocking the leak potassium channels, such as K2P channels, to depolarize the membrane (Kettunen et al., 2003). It follows that the enhanced synaptic transmission and plasticity by DAMGO could be due to an associative effect; more synapses are recruited, leading to greater depolarization of the postsynaptic membrane and greater NMDAR activation.

Activation of Astrocytic MOR Is Necessary and Sufficient for Enhancing the Glutamatergic Synaptic Transmission

Lastly, we confirmed whether astrocytic MOR is indeed critical for DAMGO-induced enhancement of synaptic transmission at SC-CA1. This DAMGO-induced increase of eEPSC was not observed in MOR-shRNA-injected CaMKIIα-Cre mice or control hGFAP-CreER^{T2} mice but was restored in tamoxifen-treated hGFAP-CreER^{T2} mice (Figures 5A–5C). Additionally, MOR-KO mice injected with the control virus (AAV-GFAP-GFP) exhibited no DAMGO-mediated increase in eEPSC amplitude (Figures 5F and 5G). On the other hand, DAMGO significantly increased the eEPSC amplitude in MOR-KO mice by means of CA1 astrocyte-specific overexpression; this enhancement was blocked by LY367385 (Figures 5D–5G). These findings together indicate that astrocytic MOR in the hippocampus is necessary and sufficient for the enhancement of synaptic transmission at SC-CA1 prompted by the binding of astrocytic glutamate to mGluR1.

The Enhanced Synaptic Transmission Leads to Synaptic Strengthening at SC-CA1

Furthermore, we tested if the enhancement of synaptic transmission induced by astrocytic MOR activation leads to strengthening of synapses at a single-cell level by performing whole-cell patch clamp to measure stimulation-evoked excitatory postsynaptic potentials (eEPSPs) under current clamp mode. Under current clamp mode, membrane potential is allowed to change freely, and any changes in synaptic strength should more closely reflect physiological conditions. We found that DAMGO caused a long-lasting increase in the amplitude of

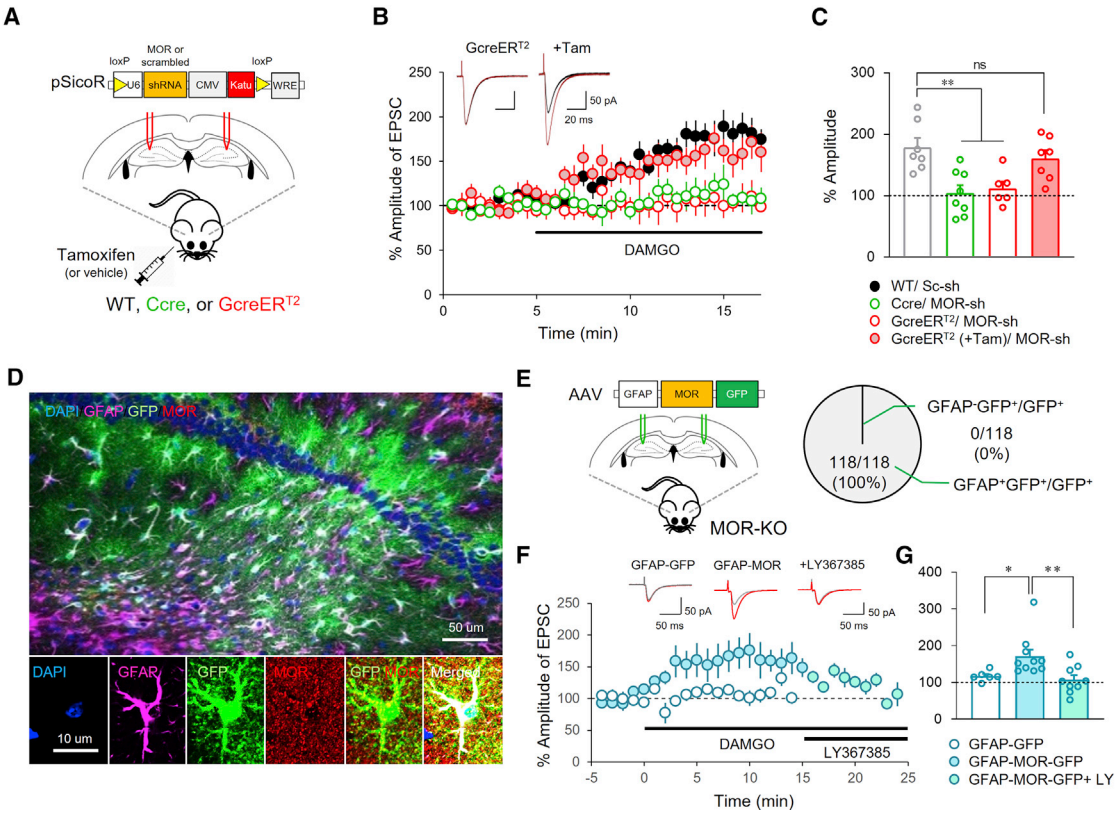

Figure 5. Astrocytic MOR Activation Is Necessary and Sufficient to Enhance Synaptic Transmission at SC-CA1

(A) Experimental scheme of mice preparation.

(B) Time course of eEPSC amplitude by bath application of DAMGO (1 μM). Representative traces of eEPSC are recorded from the CA1 pyramidal neurons of GFAP-CreER^{T2} mice with and without tamoxifen treatment.

(C) Summary bar graph of averaged eEPSC amplitude by DAMGO for last 3 min. (n ≥ 3 mice; **p < 0.01, one-way ANOVA with Dunnett's multiple comparison test).

(D) Representative confocal images of MOR over-expression in hippocampal astrocytes of MOR-KO mice.

(E) Schematic diagram of GFAP-MOR over-expression (left) and confirmation of astrocyte-specificity (right).

(F) Time courses of eEPSC amplitude in hippocampal CA1 neuron during DAMGO (1 μM) application. Insets, representative traces from each group.

(G) Summary bar graph of mean percent of amplitude of DAMGO-induced increase of eEPSC (n ≥ 3 mice; *p < 0.05, **p < 0.01, one-way ANOVA with Tukey's multiple comparison test). Data are represented as mean ± SEM.

See Table S1 for detailed description about statistical analyses.

eEPSP over a period of 30 min, which was eliminated in MOR KO mice, by the pre-treatment of APV (25 μM) or LY367385 (100 μM) (Figures 6A–6C) or by the treatment of CTOP (Figures S7A and S7B). These findings indicate that mGluR1 and NMDAR mediate synaptic potentiation upon MOR activation. Moreover, DAMGO-induced eEPSP potentiation was not observed in MOR-shRNA-injected CaMKIIα-Cre mice and control hGFAP-CreER^{T2} mice (Figures 6D–6F). However, when MOR-shRNA was injected into the tamoxifen-treated hGFAP-CreER^{T2} mice, the potentiation of eEPSP by DAMGO was significantly rescued (Figures 6D–6F). These findings indicate that astrocytic MOR is responsible for DAMGO-induced synaptic potentiation. These findings were consistent with those obtained from fEPSP recordings (Figure 2). Our findings, therefore, indicate that the activation of astrocytic MOR lowers LTP threshold at SC-CA1 synapse of dorsal hippocampus by enhancing synaptic transmission and synaptic strength.

Activation of Hippocampal Astrocytic hM4Di Causes CPP and Lowers LTP Threshold

We then investigated whether astrocytic MOR-dependent CPP can be recapitulated by the activation of hippocampal astrocytic Gi-GPCR. We virally expressed hM4Di, a Gi-coupled designer receptor (Roth, 2016), exclusively in CA1 hippocampal astrocytes by using a GFAP promoter and activated by clozapine-N-oxide (CNO) (Figures 7A–7C and S2B). The i.p. injection of CNO (2 mg/kg, i.p.) was sufficient to induce CPP in hM4Di-expressed mice but not in the control-virus-injected mice (Figure 7D). These results indicate that an activation of astrocytic Gi-GPCR is sufficient for CPP.

We further explored whether activation of astrocytic Gi-GPCR is sufficient to lower the LTP threshold. We virally expressed hM4Di in CA1 astrocytes (Figure 7E) and found that CNO application itself did not cause LTP at SC-CA1. However, CNO application coupled with 40-Hz stimulation induced LTP in the

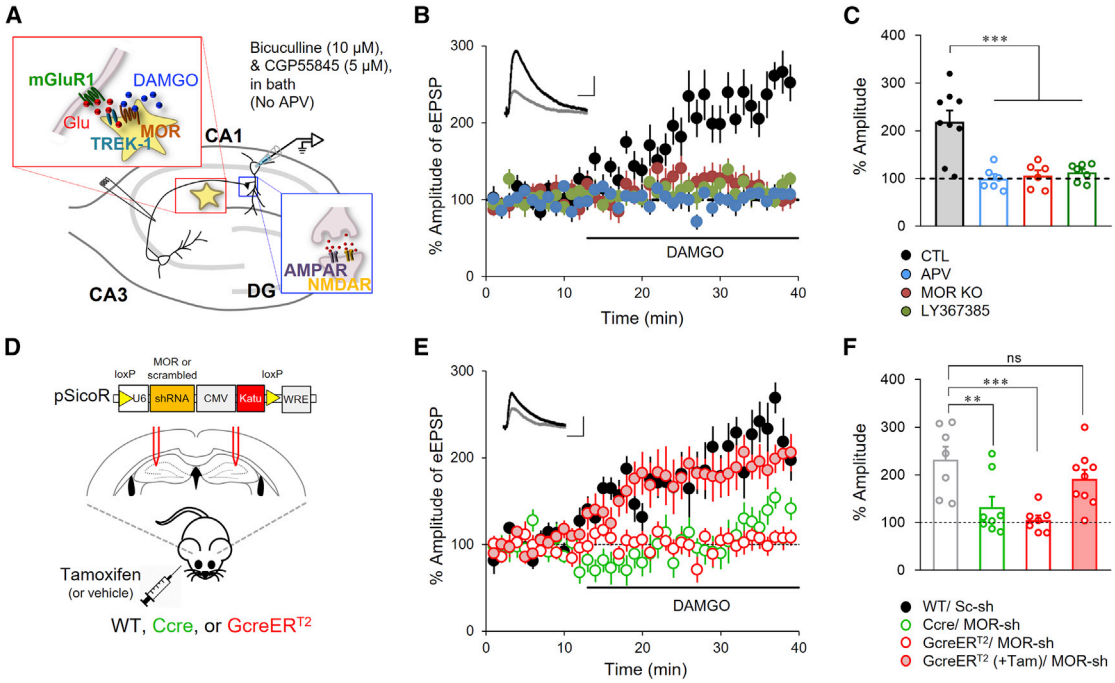

Figure 6. Astrocytic Glutamate upon MOR Activation Enhances Synaptic Strength by mGluR1 and NMDAR

(A) Mechanistic model of how astrocytic glutamate enhances synaptic strength at SC-CA1.

(B) Time courses of eEPSP amplitude by bath application of 1 μM DAMGO. Inset, representative traces before (gray) and after (black) DAMGO treatment.

(C) Summary bar graph of averaged eEPSP amplitude by 1 μM DAMGO for last 5 min (n ≥ 3 mice; ***p < 0.001, one-way ANOVA with Dunnett's multiple comparison test).

(D) Experimental scheme of mice preparation.

(E) Time courses of eEPSP amplitude by bath application of 1 μM DAMGO from each condition. Inset, representative traces of eEPSP before (gray) and after (black) DAMGO treatment in scrambled-shRNA-injected WT mice.

(F) Summary bar graph of averaged eEPSP amplitude by 1 μM DAMGO for last 5 min in each condition (n ≥ 3 mice; **p < 0.01, ***p < 0.001, one-way ANOVA with Dunnett's multiple comparison test). Data are represented as mean ± SEM.

See Table S1 for detailed description about statistical analyses.

AAV-GFAP-hM4Di-mCherry-injected hippocampus but not in control-virus-injected hippocampus (Figures 7F and 7G). Taken together, our results indicate that activation of astrocytic Gi-GPCR is necessary and sufficient to lower the threshold for LTP induction. After three decades past, our results finally provide direct evidence for the possibility of glial Gi-GPCR-mediated LTP in hippocampus (Goh and Pennefather, 1989).

DISCUSSION

In summary, we have demonstrated that activation of astrocytic Gi-GPCR, especially MOR, in the dorsal hippocampus causes glutamate release through TREK-1- and TWIK-1-containing K2P channels, increases the release probability by neuronal presynaptic mGluR1 activation, and potentiates NMDAR-dependent synaptic plasticity at SC-CA1 pathway, thus accounting for the acquisition of memory associated with CPP (Figure 7H). Although the retrieval of CPP memory was recently demonstrated to be dependent on a circuit between the dorsal subiculum and the medial entorhinal cortex layer 5 of the hippocampus (Roy et al., 2017), the molecular and cellular mechanisms underlying CPP memory acquisition have hitherto remained unknown. The present study provides a series of evidence for cellular and molecular mechanisms of CPP memory acquisition through the unexpected transduction of astrocytic inhibitory Gi signaling to prompt excitation of glutamatergic SC-CA1 synapses by astrocytic glutamate release. This mechanism of CPP through hippocampal astrocytes should provide a plausible explanation for the apparent conflict on the role of dopamine in CPP; although the mesocorticolimbic dopamine system is known to be critical for CPP, dopamine-deficient mice exhibit normal CPP (Hnasko et al., 2005). It is possible that the hippocampal astrocytic Gi-GPCR system is critical for the liking and/or pleasure and learning and/or memory aspects of CPP, whereas the mesocorticolimbic dopamine system is critical for the wanting and/or motivation aspect of CPP.

Our study does not exclude the role of mesocorticolimbic dopamine system in CPP caused by astrocytic MOR activation. Instead, our study raises a possibility that hippocampal activation by astrocytic glutamate causes context-dependent opioid reward, which may result from the NMDAR-mediated synaptic potentiation in the hippocampus. Consistent with this possibility, it has been shown that the hippocampal stimulation elevates nucleus accumbens (NAc) dopamine by activating ventral tegmental area (VTA) dopaminergic neurons (Legault et al., 2000). Moreover, overexpression of MOR in Pdyn-positive cells,

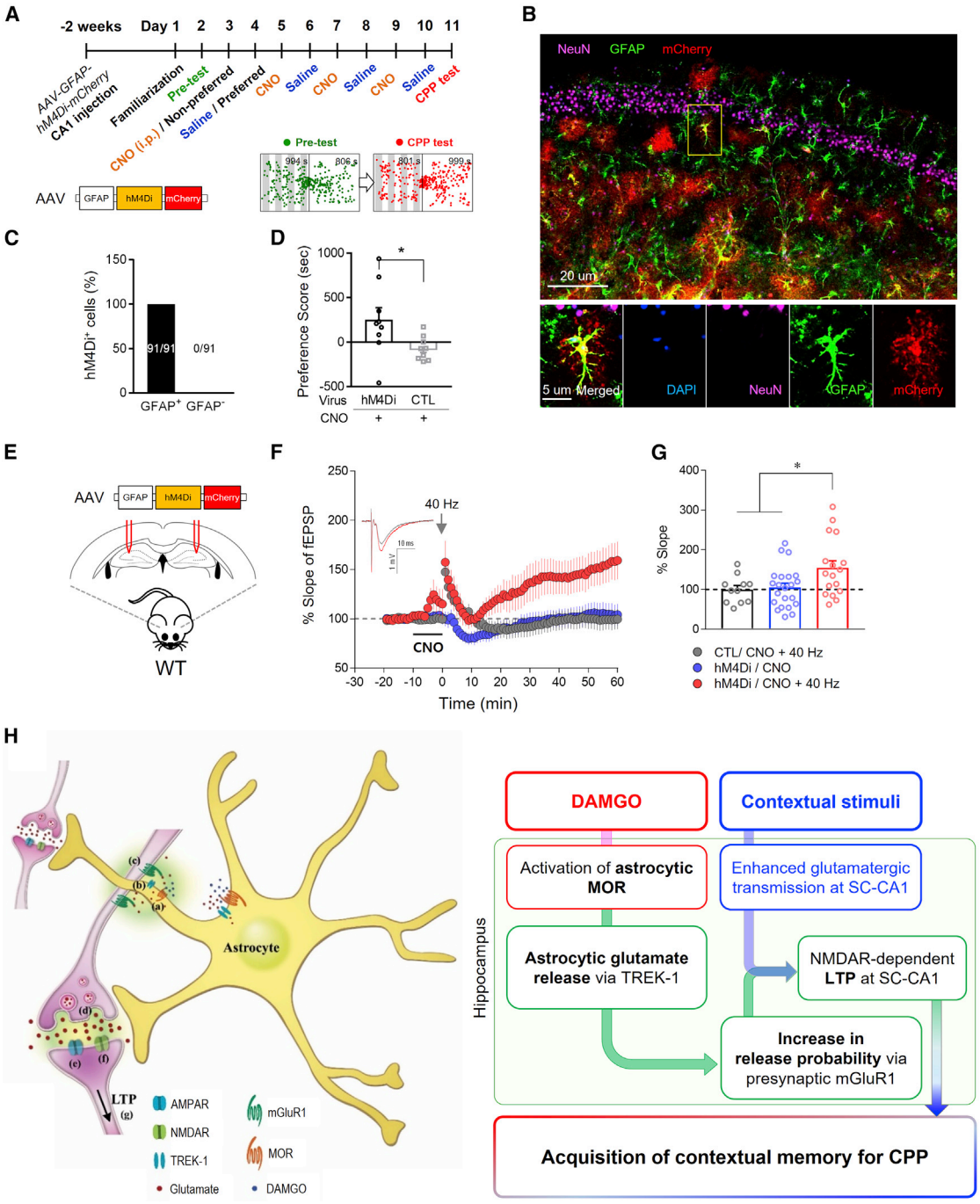

Figure 7. Activation of Astrocytic hM4Di Recapitulates Astrocytic MOR-Dependent CPP and LTP

(A) Experimental scheme and example trace of CPP test using chemogenetic activation of astrocytic Gi-GPCR.

(B) A representative confocal image of GFAP$^+$ astrocyte-specific expression of hM4Di in hippocampal CA1.

(C) Quantification of astrocyte-specific hM4Di expression.

(D) Summary bar graph of the preference score (sec) induced by chemogenetic activation of astrocytic Gi-GPCR (n = 9 mice; *$p < 0.05$, unpaired two-tailed t test with Welch's correction).

(E) Experimental scheme of astrocyte-specific expression of hM4Di.

(F) Time course of the percent fEPSP slope in each condition. Inset, example traces of hM4Di + CNO + 40 Hz group before (grey) and after (red) stimulation.

(G) Summary bar graph of the mean percent fEPSP slope for last 10 min (n $\geq$ 3 mice; *$p < 0.05$, one-way ANOVA with Tukey's multiple comparison test).

(H) Schematic model of contextual memory formation for CPP through activation of astrocytic Gi-GPCR. Data are represented as mean ± SEM.

See Table S1 for detailed description about statistical analyses.

which include not only striatal D1 neurons but also hippocampal cells, has been reported to be sufficient to cause CPP (Cui et al., 2014). Therefore, these findings strongly suggest that the hippocampus could contribute to the reward circuit as an upstream component that might activate the downstream mesocorticolimbic dopamine system.

We have shown that DAMGO treatment lowers the threshold for LTP, which is a direct result of the DAMGO-induced enhanced synaptic transmission in CA1 hippocampus. It is intriguing that activation of astrocytic MOR, $GABA_B$, and CB1, which are all Gi-GPCRs, commonly enhances synaptic transmission and plasticity (Nagai et al., 2019; Perea et al., 2016; Robin et al., 2018). However, the detailed mechanisms for each Gi-GPCR appear to diverge. Based on our findings, it is likely that astrocytic MOR behaves as a classical Gi-GPCR with no increase in cytosolic Ca^{2+} upon activation by DAMGO in hippocampal astrocytes (Figure 3; Woo et al., 2018). However, future investigation is needed to confirm that MOR is indeed coupled to Gi/o protein in astrocytes. In contrast, astrocytic $GABA_B$ and CB1 have been reported to behave non-canonically, with a robust increase in cytosolic Ca^{2+} upon activation in hippocampal astrocytes (Perea et al., 2016; Robin et al., 2018). Moreover, the excitatory effect of hippocampal astrocytic $GABA_B$ is mediated by glutamate release from astrocytes (Perea et al., 2016), whereas the effect of CB1 is mediated by D-serine (Robin et al., 2018). Furthermore, a recent report demonstrated that activation of striatal astrocytic $GABA_B$ causes an increase in cytosolic Ca^{2+} and subsequent increases in the excitatory synapse number and the synaptic transmission through an upregulation of the synaptogenic cue in striatum (Nagai et al., 2019). These findings suggest that various astrocytic Gi-GPCRs are linked to distinct signaling pathways depending on the type of Gi-GPCRs. These findings also highlight the astrocytic diversity in different brain regions as the hippocampal astrocytes display distinct functional properties that are profoundly different from striatal astrocytes. It would be very interesting to identify the downstream signaling molecules and molecular markers for the region-specific diversity of astrocytes in the future.

The critical contribution of astrocytes to hippocampal synaptic plasticity has been suggested in the past (Henneberger et al., 2010; Navarrete et al., 2012; Perea and Araque, 2007; Yang et al., 2003); the exact molecular mechanism, however, has not been elucidated. Especially, the role of astrocytic Gq-GPCR in hippocampal LTP has been controversial; optogenetic activation of astrocytic hM3Dq was recently reported to induce *de novo* synaptic potentiation (Adamsky et al., 2018), whereas it has been also reported that hippocampal LTP is not always modulated by astrocytic Ca^{2+} signaling, the key component of Gq-GPCR signaling (Agulhon et al., 2010; Fiacco and McCarthy, 2018; see however Savtchouk and Volterra, 2018). The contribution of astrocytic Gs-GPCR to hippocampal LTP and contextual memory formation has not been explored yet. Meanwhile, the possibility of glial Gi-GPCR's contribution to hippocampal LTP was initially proposed three decades ago (Goh and Pennefather, 1989) but has been forgotten. Our study unravels the critical role of astrocytic Gi-GPCR in hippocampal LTP, the neural correlate of contextual memory that is responsible for CPP.

In the current study, we demonstrate that activation of astrocytic MOR by exogenous opioids is sufficient for CPP induction. Based on the recent findings that endogenous opioids, such as β-endorphin, can be released from proopiomelanocortin (POMC)-expressing neurons in the hippocampus (Overstreet et al., 2004; Shen et al., 2016), our study raises a possibility that astrocytic MOR might be also responsible for the acquisition of contextual memory associated with pleasure. In addition to β-endorphin, other POMC-derived neuropeptides such as α-melanocyte-stimulating hormone, adrenocorticotropic hormone, and met-enkephalin might also be involved in establishment of CPP. Given the fact that a subpopulation of not only CA3 neurons but also dentate granule neurons is known to express POMC (Overstreet et al., 2004), it would also be worthwhile to investigate the possible role of astrocytic MOR in mossy fiber-to-CA3 synapses in opioid-induced CPP. These exciting possibilities await future investigations.

STAR★METHODS

Detailed methods are provided in the online version of this paper and include the following:

- KEY RESOURCES TABLE
- LEAD CONTACT AND MATERIALS AVAILABILITY
- EXPERIMENTAL MODEL AND SUBJECT DETAILS
  - Animals
- METHOD DETAILS
  - Chemogenetic activation
  - Virus injection
  - Cannula implantation
  - Conditioned place preference test
  - Passive avoidance test
  - Immunohistochemistry
- ELECTRON MICROSCOPIC IMMUNOHISTOCHEMISTRY
  - Hippocampal slice preparation
  - Glutamate and calcium imaging
  - Electrophysiology
  - Measurement of drug concentration in mouse brain
  - Cresyl violet staining
- QUANTIFICATION AND STATISTICAL ANALYSIS
  - IHC data analysis
  - Imaging data analysis
  - Statistical analysis

SUPPLEMENTAL INFORMATION

Supplemental Information can be found online at https://doi.org/10.1016/j.celrep.2019.06.071.

ACKNOWLEDGMENTS

This study was supported by the Creative Research Initiative Program funded by National Research Foundation (NRF) of Korea (2015R1A3A2066619) and Korea Institute of Science and Technology Institutional Program (project no. 2E26860) to C.J.L. and by the NRF of Korea (2017R1A5A2015391) to Y.C.B.

AUTHOR CONTRIBUTIONS

Conceptualization, M.-H.N., K.-S.H., and C.J.L; Investigation, M.-H.N., K.-S.H., J.L., W.W., W.K., J.Y.B., J.W., J.K., E.K., T.-Y.C., H.C., and S.-B.K.; Resources, K.D.P., S.-Y.C., Y.C.B., and C.J.L.; Writing - original draft preparation, M.-H.N. and K.-S.H.; Writing - review and editing, M.-H.N., K.-S.H., and C.J.L.

DECLARATION OF INTERESTS

The authors declare no completing interest.

Received: January 11, 2019
Revised: May 22, 2019
Accepted: June 20, 2019
Published: July 30, 2019; corrected online: October 5, 2019

REFERENCES

Adamsky, A., Kol, A., Kreisel, T., Doron, A., Ozeri-Engelhard, N., Melcer, T., Refaeli, R., Horn, H., Regev, L., Groysman, M., et al. (2018). Astrocytic Activation Generates De Novo Neuronal Potentiation and Memory Enhancement. Cell *174*, 59–71.e14.

Agulhon, C., Fiacco, T.A., and McCarthy, K.D. (2010). Hippocampal short- and long-term plasticity are not modulated by astrocyte Ca2+ signaling. Science *327*, 1250–1254.

Amano, T., Duvarci, S., Popa, D., and Paré, D. (2011). The fear circuit revisited: contributions of the basal amygdala nuclei to conditioned fear. J. Neurosci. *31*, 15481–15489.

Belluzzi, J.D., and Stein, L. (1977). Enkephalin may mediate euphoria and drive-reduction reward. Nature *266*, 556–558.

Bliss, T.V., and Collingridge, G.L. (1993). A synaptic model of memory: long-term potentiation in the hippocampus. Nature *361*, 31–39.

Carr, G.D., Fibiger, H.C., and Phillips, A.G. (1989). The Neuropharmacological Basis of Reward (Clarendon Press).

Casper, K.B., Jones, K., and McCarthy, K.D. (2007). Characterization of astrocyte-specific conditional knockouts. Genesis *45*, 292–299.

Chai, H., Diaz-Castro, B., Shigetomi, E., Monte, E., Octeau, J.C., Yu, X., Cohn, W., Rajendran, P.S., Vondriska, T.M., Whitelegge, J.P., et al. (2017). Neural Circuit-Specialized Astrocytes: Transcriptomic, Proteomic, Morphological, and Functional Evidence. Neuron *95*, 531–549.e539.

Chen, T.W., Wardill, T.J., Sun, Y., Pulver, S.R., Renninger, S.L., Baohan, A., Schreiter, E.R., Kerr, R.A., Orger, M.B., Jayaraman, V., et al. (2013). Ultrasensitive fluorescent proteins for imaging neuronal activity. Nature *499*, 295–300.

Conquet, F., Bashir, Z.I., Davies, C.H., Daniel, H., Ferraguti, F., Bordi, F., Franz-Bacon, K., Reggiani, A., Matarese, V., Condé, F., et al. (1994). Motor deficit and impairment of synaptic plasticity in mice lacking mGluR1. Nature *372*, 237–243.

Cui, Y., Ostlund, S.B., James, A.S., Park, C.S., Ge, W., Roberts, K.W., Mittal, N., Murphy, N.P., Cepeda, C., Kieffer, B.L., et al. (2014). Targeted expression of μ-opioid receptors in a subset of striatal direct-pathway neurons restores opiate reward. Nat. Neurosci. *17*, 254–261.

Derrick, B.E., and Martinez, J.L., Jr. (1994). Opioid receptor activation is one factor underlying the frequency dependence of mossy fiber LTP induction. J. Neurosci. *14*, 4359–4367.

Drdla, R., Gassner, M., Gingl, E., and Sandkühler, J. (2009). Induction of synaptic long-term potentiation after opioid withdrawal. Science *325*, 207–210.

Durkee, C.A., Covelo, A., Lines, J., Kofuji, P., Aguilar, J., and Araque, A. (2019). $G_{i/o}$ protein-coupled receptors inhibit neurons but activate astrocytes and stimulate gliotransmission. Glia *67*, 1076–1093.

Engelman, H.S., and MacDermott, A.B. (2004). Presynaptic ionotropic receptors and control of transmitter release. Nat. Rev. Neurosci. *5*, 135–145.

Fakira, A.K., Massaly, N., Cohensedgh, O., Berman, A., and Morón, J.A. (2016). Morphine-Associated Contextual Cues Induce Structural Plasticity in Hippocampal CA1 Pyramidal Neurons. Neuropsychopharmacology *41*, 2668–2678.

Fiacco, T.A., and McCarthy, K.D. (2018). Multiple Lines of Evidence Indicate That Gliotransmission Does Not Occur under Physiological Conditions. J. Neurosci. *38*, 3–13.

Gil-Sanz, C., Delgado-García, J.M., Fairén, A., and Gruart, A. (2008). Involvement of the mGluR1 receptor in hippocampal synaptic plasticity and associative learning in behaving mice. Cereb. Cortex *18*, 1653–1663.

Goh, J.W., and Pennefather, P.S. (1989). A pertussis toxin-sensitive G protein in hippocampal long-term potentiation. Science *244*, 980–983.

Gómez-Gonzalo, M., Navarrete, M., Perea, G., Covelo, A., Martín-Fernández, M., Shigemoto, R., Luján, R., and Araque, A. (2015). Endocannabinoids Induce Lateral Long-Term Potentiation of Transmitter Release by Stimulation of Gliotransmission. Cereb. Cortex *25*, 3699–3712.

Hawkes, C.H. (1992). Endorphins: the basis of pleasure? J. Neurol. Neurosurg. Psychiatry *55*, 247–250.

Henneberger, C., Papouin, T., Oliet, S.H., and Rusakov, D.A. (2010). Long-term potentiation depends on release of D-serine from astrocytes. Nature *463*, 232–236.

Hennig, J., Laschefski, U., and Opper, C. (1994). Biopsychological changes after bungee jumping: beta-endorphin immunoreactivity as a mediator of euphoria? Neuropsychobiology *29*, 28–32.

Heurteaux, C., Guy, N., Laigle, C., Blondeau, N., Duprat, F., Mazzuca, M., Lang-Lazdunski, L., Widmann, C., Zanzouri, M., Romey, G., and Lazdunski, M. (2004). TREK-1, a K+ channel involved in neuroprotection and general anesthesia. EMBO J. *23*, 2684–2695.

Hnasko, T.S., Sotak, B.N., and Palmiter, R.D. (2005). Morphine reward in dopamine-deficient mice. Nature *438*, 854–857.

Hwang, E.M., Kim, E., Yarishkin, O., Woo, D.H., Han, K.S., Park, N., Bae, Y., Woo, J., Kim, D., Park, M., et al. (2014). A disulphide-linked heterodimer of TWIK-1 and TREK-1 mediates passive conductance in astrocytes. Nat. Commun. *5*, 3227.

Johnson, S.W., and North, R.A. (1992). Opioids excite dopamine neurons by hyperpolarization of local interneurons. J. Neurosci. *12*, 483–488.

Kettunen, P., Hess, D., and El Manira, A. (2003). mGluR1, but not mGluR5, mediates depolarization of spinal cord neurons by blocking a leak current. J. Neurophysiol. *90*, 2341–2348.

Kringelbach, M.L., and Berridge, K.C. (2010). The Neuroscience of Happiness and Pleasure. Soc. Res. (New York) *77*, 659–678.

Lee, C.J., Bardoni, R., Tong, C.K., Engelman, H.S., Joseph, D.J., Magherini, P.C., and MacDermott, A.B. (2002). Functional expression of AMPA receptors on central terminals of rat dorsal root ganglion neurons and presynaptic inhibition of glutamate release. Neuron *35*, 135–146.

Lee, C.J., Labrakakis, C., Joseph, D.J., and Macdermott, A.B. (2004). Functional similarities and differences of AMPA and kainate receptors expressed by cultured rat sensory neurons. Neuroscience *129*, 35–48.

Legault, M., Rompré, P.P., and Wise, R.A. (2000). Chemical stimulation of the ventral hippocampus elevates nucleus accumbens dopamine by activating dopaminergic neurons of the ventral tegmental area. J. Neurosci. *20*, 1635–1642.

Marvin, J.S., Borghuis, B.G., Tian, L., Cichon, J., Harnett, M.T., Akerboom, J., Gordus, A., Renninger, S.L., Chen, T.W., Bargmann, C.I., et al. (2013). An optimized fluorescent probe for visualizing glutamate neurotransmission. Nat. Methods *10*, 162–170.

Mucha, R.F., van der Kooy, D., O'Shaughnessy, M., and Bucenieks, P. (1982). Drug reinforcement studied by the use of place conditioning in rat. Brain Res. *243*, 91–105.

Nagai, J., Rajbhandari, A.K., Gangwani, M.R., Hachisuka, A., Coppola, G., Masmanidis, S.C., Fanselow, M.S., and Khakh, B.S. (2019). Hyperactivity with Disrupted Attention by Activation of an Astrocyte Synaptogenic Cue. Cell *177*, 1280–1292.e20.

Nam, M.H., Han, K.S., Lee, J., Bae, J.Y., An, H., Park, S., Oh, S.J., Kim, E., Hwang, E., Bae, Y.C., and Lee, C.J. (2018). Expression of μ-Opioid Receptor in CA1 Hippocampal Astrocytes. Exp. Neurobiol. *27*, 120–128.

Navarrete, M., Perea, G., Fernandez de Sevilla, D., Gómez-Gonzalo, M., Núñez, A., Martín, E.D., and Araque, A. (2012). Astrocytes mediate in vivo cholinergic-induced synaptic plasticity. PLoS Biol. *10*, e1001259.

Neyman, S., and Manahan-Vaughan, D. (2008). Metabotropic glutamate receptor 1 (mGluR1) and 5 (mGluR5) regulate late phases of LTP and LTD in the hippocampal CA1 region in vitro. Eur. J. Neurosci. *27*, 1345–1352.

Nie, X., Arrighi, I., Kaissling, B., Pfaff, I., Mann, J., Barhanin, J., and Vallon, V. (2005). Expression and insights on function of potassium channel TWIK-1 in mouse kidney. Pflugers Arch. *451*, 479–488.

Overstreet, L.S., Hentges, S.T., Bumaschny, V.F., de Souza, F.S., Smart, J.L., Santangelo, A.M., Low, M.J., Westbrook, G.L., and Rubinstein, M. (2004). A transgenic marker for newly born granule cells in dentate gyrus. J. Neurosci. *24*, 3251–3259.

Penn, A.C., Zhang, C.L., Georges, F., Royer, L., Breillat, C., Hosy, E., Petersen, J.D., Humeau, Y., and Choquet, D. (2017). Hippocampal LTP and contextual learning require surface diffusion of AMPA receptors. Nature *549*, 384–388.

Perea, G., and Araque, A. (2007). Astrocytes potentiate transmitter release at single hippocampal synapses. Science *317*, 1083–1086.

Perea, G., Gómez, R., Mederos, S., Covelo, A., Ballesteros, J.J., Schlosser, L., Hernández-Vivanco, A., Martín-Fernández, M., Quintana, R., Rayan, A., et al. (2016). Activity-dependent switch of GABAergic inhibition into glutamatergic excitation in astrocyte-neuron networks. eLife *5*, 5.

Phillips, R.G., and LeDoux, J.E. (1992). Differential contribution of amygdala and hippocampus to cued and contextual fear conditioning. Behav. Neurosci. *106*, 274–285.

Portugal, G.S., Al-Hasani, R., Fakira, A.K., Gonzalez-Romero, J.L., Melyan, Z., McCall, J.G., Bruchas, M.R., and Morón, J.A. (2014). Hippocampal long-term potentiation is disrupted during expression and extinction but is restored after reinstatement of morphine place preference. J. Neurosci. *34*, 527–538.

Redondo, R.L., Kim, J., Arons, A.L., Ramirez, S., Liu, X., and Tonegawa, S. (2014). Bidirectional switch of the valence associated with a hippocampal contextual memory engram. Nature *513*, 426–430.

Robin, L.M., Oliveira da Cruz, J.F., Langlais, V.C., Martin-Fernandez, M., Metna-Laurent, M., Busquets-Garcia, A., Bellocchio, L., Soria-Gomez, E., Papouin, T., Varilh, M., et al. (2018). Astroglial CB1 Receptors Determine Synaptic D-Serine Availability to Enable Recognition Memory. Neuron *98*, 935–944.e935.

Roth, B.L. (2016). DREADDs for Neuroscientists. Neuron *89*, 683–694.

Roy, D.S., Kitamura, T., Okuyama, T., Ogawa, S.K., Sun, C., Obata, Y., Yoshiki, A., and Tonegawa, S. (2017). Distinct Neural Circuits for the Formation and Retrieval of Episodic Memories. Cell *170*, 1000–1012.e1019.

Savtchouk, I., and Volterra, A. (2018). Gliotransmission: Beyond Black-and-White. J. Neurosci. *38*, 14–25.

Shen, Y., Tian, M., Zheng, Y., Gong, F., Fu, A.K.Y., and Ip, N.Y. (2016). Stimulation of the Hippocampal POMC/MC4R Circuit Alleviates Synaptic Plasticity Impairment in an Alzheimer's Disease Model. Cell Rep. *17*, 1819–1831.

Stenman, J., Toresson, H., and Campbell, K. (2003). Identification of two distinct progenitor populations in the lateral ganglionic eminence: implications for striatal and olfactory bulb neurogenesis. J. Neurosci. *23*, 167–174.

Ventura, A., Meissner, A., Dillon, C.P., McManus, M., Sharp, P.A., Van Parijs, L., Jaenisch, R., and Jacks, T. (2004). Cre-lox-regulated conditional RNA interference from transgenes. Proc. Natl. Acad. Sci. USA *101*, 10380–10385.

Whitlock, J.R., Heynen, A.J., Shuler, M.G., and Bear, M.F. (2006). Learning induces long-term potentiation in the hippocampus. Science *313*, 1093–1097.

Wise, R.A. (2004). Dopamine, learning and motivation. Nat. Rev. Neurosci. *5*, 483–494.

Woo, D.H., Han, K.S., Shim, J.W., Yoon, B.E., Kim, E., Bae, J.Y., Oh, S.J., Hwang, E.M., Marmorstein, A.D., Bae, Y.C., et al. (2012). TREK-1 and Best1 channels mediate fast and slow glutamate release in astrocytes upon GPCR activation. Cell *151*, 25–40.

Woo, D.H., Bae, J.Y., Nam, M.-H., An, H., Ju, Y.H., Won, J., Choi, J.H., Hwang, E.M., Han, K.-S., Bae, Y.C., and Lee, C.J. (2018). Activation of Astrocytic μ-opioid Receptor Elicits Fast Glutamate Release Through TREK-1-Containing K2P Channel in Hippocampal Astrocytes. Front. Cell. Neurosci. *12*, 319.

Yang, Y., Ge, W., Chen, Y., Zhang, Z., Shen, W., Wu, C., Poo, M., and Duan, S. (2003). Contribution of astrocytes to hippocampal long-term potentiation through release of D-serine. Proc. Natl. Acad. Sci. USA *100*, 15194–15199.

Yang, Y., Zheng, X., Wang, Y., Cao, J., Dong, Z., Cai, J., Sui, N., and Xu, L. (2004). Stress enables synaptic depression in CA1 synapses by acute and chronic morphine: possible mechanisms for corticosterone on opiate addiction. J. Neurosci. *24*, 2412–2420.

STAR★METHODS

KEY RESOURCES TABLE

REAGENT or RESOURCE	SOURCE	IDENTIFIER
Antibodies		
Chicken anti-GFAP	Millipore	Cat# ab5541; RRID: AB_177521
Mouse anti-NeuN	Millipore	Cat# MAB377; RRID: AB_2298772
Rabbit anti-MOR	Santa Cruz Biotechnology	Cat# sc-15310; RRID: AB_2156520
Rabbit anti-S100b	Novus	Cat# NB110-57478; RRID: AB_922392
Guinea pig anti-GABA	Millipore	Cat# ab175; RRID: AB_91011
Rabbit anti-mGluR1α	Millipore	Cat# AB1551; RRID: AB_90765
DAPI	Pierce	Cat# D1306; RRID: AB_2629482
Alexa-647 donkey anti-chicken	Jackson ImmunoResearch	Cat# 703-605-155; RRID: AB_2340379
Alexa-594 donkey anti-rabbit	Jackson ImmunoResearch	Cat# 711-585-152; RRID: AB_2340621
Alexa 488 donkey anti-chicken	Jackson ImmunoResearch	Cat# 703-545-155; RRID: AB_2340375
Alexa 488 donkey anti-guinea pig	Jackson ImmunoResearch	Cat# 706-545-148; RRID: AB_2340472
Alexa-647 donkey anti-mouse	Jackson ImmunoResearch	Cat# 715-605-150; RRID: AB_2340862
Bacterial and Virus Strains		
pSicoR-MORsh-Katushka	KIST virus facility	N/A
pSicoR-scrambledsh-Katushka	KIST virus facility	N/A
pSicoR-scrambledsh-mCherry	KIST virus facility	N/A
AAV-GFAP-MOR-GFP	KIST virus facility	N/A
AAV-GFAP-GFP	KIST virus facility	N/A
AAV-GFAP-SF-Venus-iGluSnFR-A184S	KIST virus facility	N/A
AAV-GFAP-GCamP6f	KIST virus facility	N/A
AAV-GFAP-hM4Di-mCherry	KIST virus facility	N/A
Chemicals, Peptides, and Recombinant Proteins		
CNO	Tocris	Cat# 4936; CAS: 34233-69-7
DAMGO	Tocris	Cat# 1171; CAS: 78123-71-4
CTOP	Tocris	Cat# 1578; CAS: 103429-31-8
Tamoxifen	Sigma aldrich	Cat# T5648; CAS: 10540-29-1
(-)-Bicuculline methobromide	Tocris	Cat# 0109; CAS: 73604-30-5
CGP55845	Tocris	Cat# 1248; CAS: 149184-22-5
D-AP5	Tocris	Cat# 0106; CAS: 79055-68-8
LY367385	Tocris	Cat# 1237; CAS: 198419-91-9
Tetrodotoxin	Tocris	Cat# 1078; CAS: 4368-28-9
Experimental Models: Organisms/Strains		
Mouse: C57BL6/J	The Jackson Laboratory	Cat# JAX: 000664
Mouse: CaMKIIα-Cre	The Jackson Laboratory	Cat# JAX: 005359
Mouse: hGFAP-CreER^{T2}	The Jackson Laboratory	Cat# JAX: 012849
Mouse: DLX-Cre	The Jackson Laboratory	Cat# JAX: 008199
Mouse: MOR-KO	The Jackson Laboratory	Cat# JAX: 007559
Mouse: B6;129S6-Gt(ROSA)26Sortm14 (CAG-tdTomato)Hze/J	The Jackson Laboratory	Cat# JAX: 007914
Mouse: mGluR1-KO	University of Maryland	N/A
Mouse: TREK-1/TWIK-1 double KO	University of Nice-Sophia Antipolis	N/A
Oligonucleotides		
MOR-shRNA targeting sequence: 5′-gac tgt ttc ctg gca ctt c-3′	KIST (Nam et al., 2018)	N/A

(*Continued on next page*)

Continued

REAGENT or RESOURCE	SOURCE	IDENTIFIER
Recombinant DNA		
pSicoR-MORsh-Katushka	This paper	N/A
pSicoR-scrambledsh-Katushka	This paper	N/A
pSicoR-scrambledsh-mCherry	This paper	N/A
AAV-GFAP-MOR-GFP	This paper	N/A
AAV-GFAP-GFP	This paper	N/A
AAV-GFAP-SF-Venus-iGluSnFR-A184S	This paper	N/A
AAV-GFAP-GCamP6f	This paper	N/A
AAV-GFAP-hM4Di-mCherry	This paper	N/A
Software and Algorithms		
GraphPad Prism 7	GraphPad software	http://www.graphpad.com/scientific-software/prism
NIS-Elements	Nikon	https://www.nikonmetrology.com/en-gb/product/nis-elements-microscope-imaging-software
ImageJ	NIH	https://imagej.nih.gov/ij/download.html
Minianalysis	Synaptosoft	http://www.synaptosoft.com/MiniAnalysis/

LEAD CONTACT AND MATERIALS AVAILABILITY

Further information and requests for resources and reagents should be directed to and will be fulfilled by the Lead Contact, C. Justin Lee (cjl@ibs.re.kr).

EXPERIMENTAL MODEL AND SUBJECT DETAILS

Animals

Wild-type, CaMKIIα-Cre, hGFAP-CreER^{T2}, and DLX-Cre mice of C57BL/6J background were used for cell type specific gene silencing system. MOR KO (Stock No. 007559) and CAGfloxStop-tdTomato (Ai14) (B6;129S6-Gt(ROSA)26Sortm14(CAG-tdTomato)Hze/J) conditional reporter line (Stock No. 007914) were obtained from Jackson Laboratory. mGluR1 KO mice were provided from University of Maryland; the generation of mGluR1 KO has been previously reported (Conquet et al., 1994). TREK-1/TWIK-1 double KO mouse line, which was generated by crossing TREK-1 KO (Heurteaux et al., 2004) and TWIK-1 KO (Nie et al., 2005), was kindly provided from Dr. Florian Lesage (University of Nice-Sophia Antipolis). We validated the mice by examining passive conductance of astrocytes (Figures S6A–S6D), as previously described (Hwang et al., 2014). For electrophysiological experiments, 7 to 8-week-old male mice were used. For primary culture of hippocampal astrocytes, P0-P3 C57BL/6J mice were used. For behavioral experiments, 12 to 14-week-old male mice were used. All animals were maintained in a vivarium with light/dark cycle (8:00 AM∼8:00 PM). Animal care and handling were performed according to the directives of the Animal Care and Use Committee and institutional guidelines of KIST (Seoul, Korea). Animals were randomly used for experiments.

METHOD DETAILS

Chemogenetic activation

We designed AAV-GFAP-hM4Di-mCherry virus to selectively express Gi-DREADD in the GFAP-positive astrocytes. We injected the virus into hippocampal CA1, 2 weeks prior to start CPP. To activate Gi-DREADD, we administered CNO at a dose of 2 mg/kg, 30 minutes prior to place the animal into the CPP chamber.

Virus injection

We used stereotaxic device to deliver a certain gene into CA1 of dorsal hippocampus (coordinates: AP −1.8 mm, ML ± 1.5 mm, DV −1.7 mm). We injected 1 to 2 μL of virus at a rate of 0.2 μL/min and waited for 1 or 2 weeks for the knockdown to occur for lentivirus or AAV virus, respectively.

Cannula implantation

Mice were kept under isoflurane anesthesia and mounted in a stereotaxic frame (David Kopf Instruments) with the upper incisor bar set at 2.5 mm below the interaural line. After exposing the skull and drilling a burr hole, a guide cannula (Plastics One) was positioned

in right and left hippocampus (AP, −1.8 mm; ML, ± 1.5 mm from bregma; DV, −1.7 mm below the dura) and secured to the skull with anchor screws and acrylic dental cement.

Conditioned place preference test

The apparatus for CPP training and testing consisted of two compartments polyvinyl chloride (PVC) boxes. One compartment (20-cm long, 20-cm wide, and 30-cm high) was black with a stainless steel grid rod floor, and another compartment was striped with black and white. Two compartments are divided by wall which has a door. When we perform CPP experiments, we used positive and negative control, simultaneously. After finishing CPP experiments, the analysis of behavior was analyzed based in a blind manner. At the end of the experiments, we confirmed the infusion site of DAMGO in the hippocampus.

Pre-conditioning (Days 1, 2)

During the preconditioning phase of the experiment, the door between two compartments was open. Mice moved around two compartments for habituation for 30 min on day 1. The time spent in each of the compartments was recorded for 30 min on day 2 to determine preferred or non-preferred compartment. If a mouse spent more than 60% of the 30 min in either the black or striped compartment, it was eliminated from further experiment.

Conditioning (Days 3-10)

For the CPP experiment with DAMGO intra-CA1 infusion, we infused 400 ng of DAMGO dissolved in 2 μL saline into the bilateral hippocampal CA1 through the cannula for 5 minutes at a rate of 0.4 μL/min just before placing the mice into non-preferred compartment of CPP chamber on days 3, 5, 7, and 9. On days 4, 6, 8, and 10, saline was infused into the bilateral hippocampal CA1 in the same way to DAMGO infusion and the mice were placed into preferred compartment. For the CPP experiment with DAMGO i.p. injection, DAMGO (1 mg/kg) or same amount of saline was intraperitoneally injected just before placing the mice into the CPP box. For the CPP experiment using CTOP, we injected 1 μL of 1 mM CTOP into bilateral hippocampal CA1, 30 minutes prior to DAMGO i.p. injection.

Post-conditioning test (Day 11)

With the chamber door open, the mouse movement was recorded for a total of 30 min. The preference score was calculated for each animal as follow: Preference score = (prefer – non-prefer)before + (non-prefer – prefer)after.

Passive avoidance test

Adult C57BL/6J mice (8 - 10 weeks old) were placed in the lighted compartment and allowed to explore for 60 s. Then the door was raised and the mouse was allowed to explore freely. The latency to enter the dark compartment with all four paws was recorded. On day 2, the latency to enter the dark compartment was similarly recorded. We delivered a foot shock (0.5 mA, 2 s duration) 3 s after the door was closed. The mouse was removed to its home cage 30 s after the foot shock. On test day (24 hr after training), the mouse was returned to the lighted compartment. After 5 s, the door was lifted, and the latency to enter the dark compartment was recorded.

Immunohistochemistry

Animals were deeply anesthetized using 2% avertin and perfused with 0.1M PBS, followed by 4% paraformaldehyde. Brains were post-fixed in 4% paraformaldehyde at 4°C for 24 hr and 30% sucrose 4°C for 48hr. Brains were then cut in coronal sections of 30 μm on a cryosection. Sections were blocked in 0.1M PBS containing 0.3% Triton X-100 (Sigma) and 2% donkey serum (Genetex) for 30 min at room temperature. Primary antibody used are as follow: chicken anti-GFAP (1:500, ab5541, Millipore), mouse anti-NeuN (1:1000, MAB377, Millipore), rabbit anti-MOR (1:200, sc-15310, Santa Cruz Biotechnology), rabbit anti-S100b (1:200, NB110-57478, Novus), and guinea pig anti-GABA (1:500, ab175, Millipore). The brain samples with primary antibodies were incubated overnight at 4°C. Then, the sections were washed three times in 0.1 M PBS and incubated in proper secondary antibodies from the Jackson Laboratory for 1.5 hr. After three rinses in 0.1 M PBS and DAPI staining at 1:3000 (PIERCE), the sections were mounted on polysine microscopic slide glass (Thermo Scientific). Images were acquired using a Nikon A1R confocal microscope. We repeated each experiment at least three times.

ELECTRON MICROSCOPIC IMMUNOHISTOCHEMISTRY

Three male Sprague-Dawley rats weighing 270 - 290 g were used. Animals were deeply anesthetized with sodium pentobarbital (80 mg/kg, i.p.) and perfused transcardially with heparinized normal saline (10 mL for mouse and 100 mL for rat), followed by freshly prepared mixture (50 mL for mouse and 500 mL for rat) of 4% paraformaldehyde and 0.01% glutaraldehyde in 0.1 M phosphate buffer (PB), pH 7.4. Hippocampus was removed and postfixed in the same fixative for 2 hours at 4°C. Sections were cut sagittally on a Vibratome at 60 μm and cryoprotected in 30% sucrose in PB overnight at 4°C. Sections were frozen on dry ice for 20 minutes, thawed in phosphate-buffered saline (PBS; 0.01 M, pH 7.2) to enhance penetration. They were pretreated with 1% sodium borohydride for 30 minutes to quench glutaraldehyde and then blocked with 3% H2O2 for 10 minutes to suppress endogenous peroxidases and with 10% normal donkey serum (NDS, Jackson ImmunoResearch, West Grove, PA) for 30 minutes to mask secondary antibody binding sites. For immunostaining for mGluR1α, sections of hippocampus pretreated as above were incubated overnight in rabbit anti-mGluR1α (1:25, AB1551, Millipore) antibody. After rinsing in PBS, sections were incubated with a biotinylated donkey anti-rabbit (1:200, Jackson ImmunoResearch) antibody for 2 - 3 hours. The sections were rinsed in PB several times, and were incubated

with ExtrAvidin peroxidase (1:5000, Sigma, St. Louis, MO) for 1 hour and the immunoperoxidase was visualized by nickel-intensified 3,3′-diaminobenzidine tetrahydrochloride (DAB). Sections were further rinsed in PB, osmicated (in 1% osmium tetroxide in PB) for 1 hour, dehydrated in graded alcohols, flat-embedded in Durcupan ACM (Fluka, Buchs, Switzerland) between strips of Aclar plastic film (EMS), and cured for 48 hours at 60°C. Chips containing prominent staining for MOR or TREK-1 or mGluR1 in the hippocampus were cut out of the wafers and glued onto blank resin blocks with cyanoacrylate. Serially cut thin sections were collected on Formvar-coated single-slot nickel grids and stained with uranyl acetate and lead citrate. Grids were examined on a Hitachi H 7500 electron microscope (Hitachi, Tokyo, Japan) at 80 kV accelerating voltage. Images were captured with Digital Micrograph software driving a cooled CCD camera (SC1000; Gatan, Pleasanton, CA, USA) attached to the microscope, and saved as TIFF files.

Hippocampal slice preparation

Animals were deeply anesthetized with isoflurane, followed by decapitation. The brains were removed from the skull and placed in an ice-cold oxygenated (95% O2 and 5% CO2) artificial cerebrospinal fluid (ACSF; 130 NaCl, 24 NaHCO3, 3.5 KCl, 1.25 NaH2PO4, 1 CaCl2, 3 MgCl2 and 10 glucose (in mM), pH 7.4). Transverse slices of 350-400 μm thickness were cut with vibrating microtome (Leica VT1000s) and stored in an incubation chamber at room temperature for at least 1 hr before recording.

Glutamate and calcium imaging

AAV-GFAP-SF-Venus-iGluSnFR-A184S or AAV-GFAP-GCamP6f virus was injected into CA1 hippocampus of 7-week old C57BL/6 mice as described above. Hippocampal slices were transferred to the recording chamber, which was constantly perfused with oxygenated ACSF composed of 130 NaCl, 24 NaHCO3, 3.5 KCl, 1.25 NaH2PO4, 1.5 CaCl2, 1.5 MgCl2 and 10 glucose (in mM) saturated with 95% O2%–5% CO2, at pH 7.4. Cells for all the experiments were imaged using Image workbench (Indec biosystems) with a 60X water-immersion objective lens with a numerical aperture of 0.9 and a 488-nm fluorescent imaging filter. Astrocytes were scanned at 0.5 to 1 frame per second for imaging sessions. The following chemicals were applied in the bath: DAMGO (1 μM), CTOP (1 μM), TTX (0.5 μM), TFLLR (30 μM). TTX and CTOP were applied in the bath at least 5 min prior to recording to allow adequate equilibration. A constant flow of fresh buffer perfused the imaging chamber at all times.

Electrophysiology

Hippocampal slices were transferred to the recording chamber as described above. For voltage clamp experiments, the solution used to fill the electrodes was composed of 140 Cs-Gluconate, 10 HEPES, 7 NaCl, 4 Mg-ATP and 0.3 Na3-GTP (in mM); the solution for current clamp recordings was composed of 140 K-Gluconate, 10 HEPES, 7 NaCl, 4 Mg-ATP and 0.3 Na3-GTP (in mM). For some experiments 0.5 μM TTX, 10 μM bicuculline, or 5 μM CGP55845 was added to the extracellular solution, extracellular Mg2+ was reduced to 5 μM.

Visually guided whole-cell patch recordings were obtained from CA1 pyramidal neuron in voltage clamp or current clamp configuration using a Multiclamp 700B amplifier (Axon Instruments, Union City) and a borosilicate patch pipette of 5 – 8 MΩ resistance. All neurons included in this study had a resting membrane potential below −55 mV, had an access resistance in the range of 20 – 60 MΩ, and showed only minimal variation in these parameters during the recordings period. Records were filtered at 2 kHz and digitized at 10 kHz using a Digidata 1322A (Axon Instruments, Union City). Synaptic responses were evoked by applying 0.1 ms current injection (50 – 200 μA) to a bipolar stimulating electrode placed in the striatum radiatum.

For field recording brains were isolated rapidly and placed in ice-cold, oxygenated dissection buffer containing 5 KCl, 1.23 NaH2PO4, 26 NaHCO3, 10 dextrose, 0.5 CaCl2, 10 MgSO4, and 212.7 sucrose (in mM). Transverse hippocampal slices were incubated in oxygenated artificial cerebrospinal fluid (ACSF) containing 124 NaCl, 5 KCl, 1.23 NaH2PO4, 2 CaCl2, 1 MgSO4, 26 NaHCO3 and 10 dextrose (in mM) at 28–30°C for at least 1 h before recording. Recordings were performed using AM-1800 microelectrode amplifier (A-M systems, Sequim), PG 4000A stimulator (Cygnus Technology, Delaware Water Gap, PA, USA), and SIU-90 isolated current source (Cygnus Technology, Delaware Water Gap). Baseline responses were collected at 0.07 Hz with a stimulation intensity that yielded a 40 – 60% maximal response. IGOR software (Wavemetrics, Lake Oswego) was used for digitizing and analyzing the responses.

Measurement of drug concentration in mouse brain

Four ICR mice with 7 to 8 weeks of age were purchased from Koatech (Korea) and maintained in pathogen-free facility at Daegu-Gyungpook Medical Inovation Foundation. Mice used in this study were fed by free access to autoclaved water and food *ad libitum*. DAMGO, which was dissolved in saline, injected into mice intraperitoneally to be 10 mg/kg and euthanized 0.25, 0.5, and 1 hr after injection. Then, brains obtained from the mice were washed with PBS three times to remove blood and homogenized in 4 volumes PBS of brain weight. 20 μL brain homogenate was added with 80 μL acetonitrile and the mixture was centrifuged at 15,000 rpm at 4°C for 5 min. Supernatant was loaded onto LC-MS/MS (TSQ Vantage Triple-Stage Quadrupole Mass Spectrometer, Thermo Scientific Fisher), and the limits of quantification (LOQ) for DAMGO ranged from 1 to 2000 ng/mL.

Cresyl violet staining

Mice were transcardially perfused with 10% formalin and then brains were extracted and fixed further in 10% formalin at room temperature. Coronal sections (50-μm thick) were cut through the entire hippocampus region using a microtome cryostat (Microm,

Germany) at −23°C. Brain slices were mounted on the slides and then stained with Cresyl Violet according to the general Nissl staining procedure. Injection sites were examined to determine whether DAMGO was injected into striatum radiatum of the CA1 hippocampus.

QUANTIFICATION AND STATISTICAL ANALYSIS

IHC data analysis

Confocal microscopic images were analyzed using the ImageJ program (NIH).

Imaging data analysis

Analyses of time-lapse image series were performed using Image Workbench. Astrocytic soma was chosen for ROIs. Time traces of fluorescence intensity were extracted from the ROIs and converted to dF/F values. The integrated area-under-curve of dF/F traces were measured using Prism 7 (GraphPad Software).

Statistical analysis

Statistical analyses were performed using Prism 7. Differences between two different groups were analyzed with the two-tailed Student's unpaired t test or Mann-Whitney test (when the data is not normally distributed). For assessment of change of a group by a certain intervention, the significance of data was assessed by the two-tailed Student's paired t test. For comparison of multiple groups, one-way analysis of variance (ANOVA) with Tukey's or Dunnett's multiple comparison test, or two-way ANOVA with Bonferroni's multiple comparison test was assessed. Data from multiple independent experiments was assumed to be normal variance. $p < 0.05$ was considered to indicate statistical significance throughout the study. The significance level is represented as asterisks ($^*p < 0.05$, $^{**}p < 0.01$, $^{***}p < 0.001$; ns, not significant). Detailed statistical analysis contents are described in Table S1. Unless otherwise specified, all data are presented as mean ± SEM. No statistical method was used to predetermine sample size. Sample sizes were determined empirically based on our previous experiences or the review of similar experiments in literatures. The numbers of animals used are described in the corresponding figure legends or on each graph. All experiments were done with at least three biological replicates. Experimental groups were balanced in terms of animal age, sex and weight. Animals were genotyped before experiments, and they were all caged together and treated in the same way. Animals were randomly and evenly allocated to each experimental group. To perform the group allocation in a blinded manner during data collection, animal preparation and experiments were performed by different investigators. Unless otherwise specified, no data point was excluded.